NJC

Accepted Manuscript

ROYAL SOCIETY OF CHEMISTRY

www.rsc.org/njc

Fabrication of Ag Nanoparticles Supported on One-Dimensional (1D) Mn$_3$O$_4$ Spinel Nanorods for Selective Oxidation of Cyclohexane at RoomTemperature

Shankha Shubhra Acharyya, Shilpi Ghosh, Sachin Kumar Sharma and Rajaram Bal*

*Catalytic Conversion & Processes Division, CSIR-Indian Institute of Petroleum, Dehradun - 248005, India. Fax: +91 135 2660202; Tel: +91135 2525 917; E-mail: raja@iip.res.in

ABSTRACT: Ag nanoparticles (with 2-5 nm size) supported on Mn$_3$O$_4$ nanorods were prepared in presence of cationic surfactant cetrimonium bromide in hydrothermal method. The material was characterized in detailed by X-Ray Diffraction, Scanning Electron Microscopy, X-ray Photoelectron Spectroscopy, Transmission Electron Microscopy, Scanning Transmission Electron Microscopy-mapping, Raman spectroscopy, Fourier-Transformed Infrared Spectroscopy and Inductively Coupled Plasma-Atomic Emission Spectroscopy. Electron microscopy studies revealed the formation of 1D nanorods morphology. XRD revealed the formation of Mn$_3$O$_4$ spinel phase and TEM showed that ultrasmall-sized metallic Ag-nanoparticles deposited on Mn$_3$O$_4$ spinel (nanorods). This Ag/Mn$_3$O$_4$ nanomaterial exhibited excellent catalytic activity in cyclohexane oxidation reaction at room temperature. The impacts of various reaction parameters (e.g. time, substrate: H$_2$O$_2$ molar ratio etc.) were investigated in detail. A detailed characterization study demonstrated the correlation between the physicochemical properties of the Ag-Mn oxide nanorods and their catalytic performance. A cyclohexane conversion of 88% with 75% cyclohexanone selectivity with an overall C$_6$ selectivity (cyclohexanol + cyclohexanone) of 100% was accomplished at room temperature. The Ag/Mn$_3$O$_4$ catalyst hardly exhibited leaching up to eight reuses, proving its true heterogeneity nature.

1

INTRODUCTION

Currently, studies on morphology-dependent catalytic-performance have drawn potential interest in the field of heterogeneous catalysis.[1-3] The architecture of catalytically active nanomaterials with precise and tunable morphology to accomplish excellent catalytic performance is of great significance. One-dimensional (1D) nanomaterials, which have been emerging under said area, are the subject of potential attention for the specific physical properties that are shown by them in comparison to their bulk counterparts.[4-6] Therefore, 1D nanomaterials have been the focus of extensive research in recent years, owing to their important applications in our daily life.[7-10] In addition, the surface of 1D nanomaterials is enriched in coordinatively unsaturated sites which play crucial role in performing high catalytic activities.[6] Various synthetic techniques have been developed for the preparation of 1D nanostructures, among which hydrothermal preparation method has been selected as the most suitable one.[11-13] The heterogeneous oxidation by Ag-based catalysts is a significant process in chemical technologies,[14-16] and in principle, the catalytic properties of AgNPs specially in oxidation reactions depend on the particles' size, as well as on the support's nature. Moreover, manganese oxide serves as an excellent support as it possesses considerable ability to activate and supply oxygen.[17] Therefore, Ag-Mn-bimetallic oxide nanostructures have been a topic of potential interest due its efficacy in super capacitance,[18] low-temperature CO oxidation,[19] catalytic oxidation of benzene,[20] toluene,[21] styrene,[22] alcohols,[17] etc. In recent years, our group reported the facile preparation of various bimetallic-1D nanomaterials,[23-26] and we came forward to synthesize 1D Ag-Mn oxide nanostructures in a facile cost-effective hydrothermal method. We report here cetrimonium bromide (CTAB)-promoted synthesis of ultrasmall Ag nanoparticles supported on Mn_3O_4 spinel nanorods in hydrothermal route. The process is highly reproducible, can be prepared in a large scale (~50 g) and can be preserved for times. Although there have been several reports on Ag-Mn nanocomposites, cationic surfactant CTAB-mediated formation of throughout uniform Ag-Mn nanorods (where supported Ag nanoparticles are ~3.5 nm) in hydrothermal method with high aspect ratio is not reported, to date.

The selective catalytic oxidation of saturated hydrocarbons is one of the most challenging subjects in recent heterogeneous catalytic chemistry owing to the huge economic benefit from fine chemicals production.[27] The selective oxidation of cyclohexane, has been emerging under this area, is of potential interest because its product, KA-oil (cyclohexanone + cyclohexanol), is crucial intermediate in manufacturing Nylon-6 and Nylon-66.[28,29] Since the products, (KA oil), are more reactive than the mother-reactant cyclohexane, high selectivity (about 80%) to KA-oil is obtained only at very poor cyclohexane conversion (only about 5%) using homogeneous cobalt catalysts in the current industrial process; moreover, high reaction temperature (>150 °C) is needed here. Furthermore, several unwanted by-products are generated in this process.[30] This low conversion and selectivity, leaching of metal, and over-oxidation of products in the existing catalytic systems reinforce the need for new systems using reinforce the need for new catalytic systems, including heterogeneous catalyst and clean oxidant. Therefore, nowadays, development of ultimate catalytic systems with the perfect performances (100% yield) for the sake of environmentally friendly green process, is highly demanding.[31] To overcome this problem, many researchers came forward and applied certain oxidants like tert-butyl hydroperoxide (TBHP),[32] H_2O_2,[33] and molecular O_2.[34] Although oxidation of cyclohexane with the greenest oxidant molecular oxygen have displayed significant progress, but their applications are limited; either H_2O_2 or TBHP and even *N*-hydroxyphthalimide (NHPI) was used as co-catalyst to accelerate the initiation step of the oxidation or huge amount of organic solvent was used. That's why, the technology with which cycloalkanes has been oxidized by molecular oxygen to generate their corresponding oxygenates has not been developed well up to now. Therefore, a mammoth task in this field is to design the heterogeneous catalyst that affords the primary product with high yield. Our previous report showed that, Cu (II) nanoclusters supported on nanocrystalline Cr_2O_3[35] and $CuCr_2O_4$ spinel nanoparticles[36] catalysts efficiently converts cyclohexane to cyclohexanone but, the former catalyst suffers severe leaching and the latter one suffers from furnishing high yield of product; therefore a catalyst that is devoid of leaching properties is highly demanding in case of liquid phase reactions, since the efficacy of a heterogeneous catalyst is elucidated in terms of its reusability

Herein, we report the selective oxidation of cyclohexane to cyclohexanone using H_2O_2 as oxidant using our so prepared Ag-Mn catalyst with unique 1D structure. A cyclohexane conversion of 88%, with a cyclohexanone conversion of 75% was achieved at room temperature (40 °C). To the best of our knowledge, there is no literature that reports cyclohexane oxidation with such a high yield of cyclohexanone using highly recyclable Ag-Mn catalyst with unique 1D structure.

EXPERIMENTAL

Materials and Methods. Anhydrous manganese chloride, silver nitrate, cetrimonium bromide (CTAB, 99%), solution of hydrazine monohydrate, cyclohexane, acetonitrile and H_2O_2 (50%) were purchased from Sigma Aldrich. Absolute ethanol (AR ACS for Analysis) from Fisher Scientific was bought. NH_3 solution was bought from Acros Organics. Deionized water (HPLC grade) was used in the synthesis.

Catalyst Preparation. In a typical synthesis method, 8.24 g anhydrous manganese (II) chloride ($MnCl_2$) was dissolved in 15g water to give a clear solution. The pH of solutions was measured by pH Meter, which was standardized for pH measurement prior to use. By gradual addition of few drop ammonia solution, the pH of the solution was made 8; the colour of the solution became pinkish to brownish gradually. Then 30% ethanolic solution of CTAB (5.07 g) + $AgNO_3$ (0.47) g was added dropwise (taking 6% Ag-loading on Mn_3O_4 spinel), followed by intensive stirring for 2h. A solution of hydrazine monohydrate (80% aqueous solution) was added drop wise to the well stirred mixture at RT. All the reagents were used maintaining the ratio: Ag: CTAB: hydrazine: H_2O = 1: 5: 1.5: 300. The mixture was stirred for 30 min. After 30 min stirring, the mixture was treated hydrothermally at 180 °C for 18 h; after 18 h, the autoclave was cooled to RT and, the so obtained thick brown solid products were collected by means of centrifugation at 7500 rpm and washed with water and ethanol several times before drying in argon at 100 °C for 10 h under vacuum. The resulting dry powder was undergone calcinations which were operated at 500 °C in argon at ramp of 1 °C min^{-1}.

Liquid-Phase Oxidation. Catalytic liquid phase oxidation of cyclohexane was carried out using a two neck 25 ml round bottom flask attached with a condenser, thermometer and a magnetic stirrer. In a typical liquid-phase reaction, 15 ml acetonitrile, 1 g cyclohexane and 0.1 g Ag-Mn catalyst were taken in the flask. The reaction was operated at room temperature (40 °C). Then 3.3g H_2O_2 (50% aq. solution) was added dropwise. Small aliquots of the sample were withdrawn from the reaction mixture at regular intervals for analysis using a syringe. After completion of the reaction, the solid particles (catalyst) were separated and the products were analysed by Gas Chromatograph (GC, Agilent 7890) equipped with a flame ionization detector (FID) and a HP5 capillary column (30m length, 0.28 mm id, 0.25µm film thickness) using methanol as internal standard. The product identification was carried out by injecting the reference samples and with GC-MS.

RESULTS AND DISCUSSIONS

Catalyst Characterization. The 1D Ag-Mn rod-like nanocomposite was synthesized following our own preparation method,[23-26] taking nitrate precursor of Ag and Mn, and was characterized by XRD, XPS, SEM, TEM, STEM-mapping, Raman-spectroscopy, FTIR, BET surface area and ICP-AES. The typical X-ray-diffraction (XRD) diagram of the Ag-Mn catalyst are shown in Figure 1. The XRD diffractogram showed the peaks at 2θ= 28.8°, 36.08°, 44.4°, 59.8°, 69.6° etc. which can be indexed to Hausmannite-type tetragonal Mn_3O_4 with specific group $I4_1/amd$ [JCPDS 24-0734], with a maximum intensity at 36.085 (indicative of (211) plane of Mn_3O_4) and no other impurities owing to other oxides of Mn can be observed, which unveiled the highly phase-purity of the synthetic procedure. However, very small XRD peaks corresponding to metallic silver (i.e. Ag (0)) was observed, demonstrating either very small particle size of Ag-species or low Ag-loading is present in the sample. However, when Ag loading was increased to 7.8 %, some sorts of Ag peaks were clearly visible in the XRD diffractogram (Figure S1, Supporting Information). The XRD pattern of the spent catalyst was indicate that the catalyst remains unchanged even after 8 reuses.
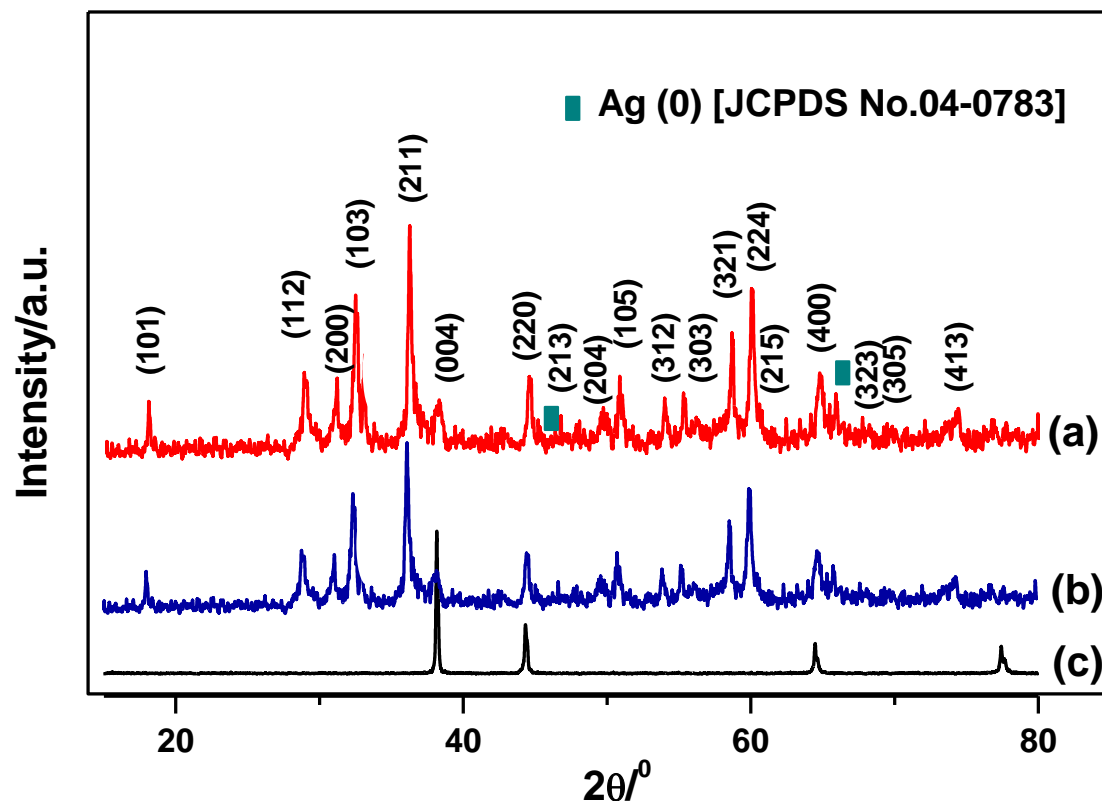
Fig. 1 XRD patterns of (a) fresh and (b) spent 1D Ag-Mn nano-rod catalyst and that of commercial (c) Ag.

The indication of metallic silver present in the fresh catalyst was confirmed from X-ray photoelectron spectroscopy (XPS) analyses. The binding energy values of 368.3 eV and 374.3 eV demonstrated the presence of Ag $3d_{5/2}$ and Ag $3d_{3/2}$ (Figure 2)[24-26,37] respectively. It can be observed from the XPS spectra of Mn in the sample (Figure S2 & S3, Supporting Information) showed that, that the Mn 2p peak consists of two main spin-orbital lines. The binding energies 641.46 eV and 653.13 eV indicated the presence of Mn $2p_{3/2}$ and Mn 2p1/2. These binding energies bear splitting of 11.4 eV, which are in good agreements with the earlier reports.[38,39] Deconvolution of Mn 2p spectrum was displayed as two pairs of doublets: 641.56 and 643.64

eV, 652.88 and 654.75 eV, corresponding to Mn^{3+} $2p_{3/2}$ and $Mn^{2+}2p_{3/2}$, Mn^{3+} $2p_{1/2}$ and $Mn^{2+}2p_{1/2}$, respectively. The calculated ratio of Mn^{2+}: Mn^{3+} is around 1:2 (Table S1, Supporting Information), which is in agreement with a previously reported value.[39,40] The Ag 3d binding energy of the spent catalyst was observed at 368.3 eV, demonstrating the fact that metallic silver remained unhindered during catalysis.[24-26]
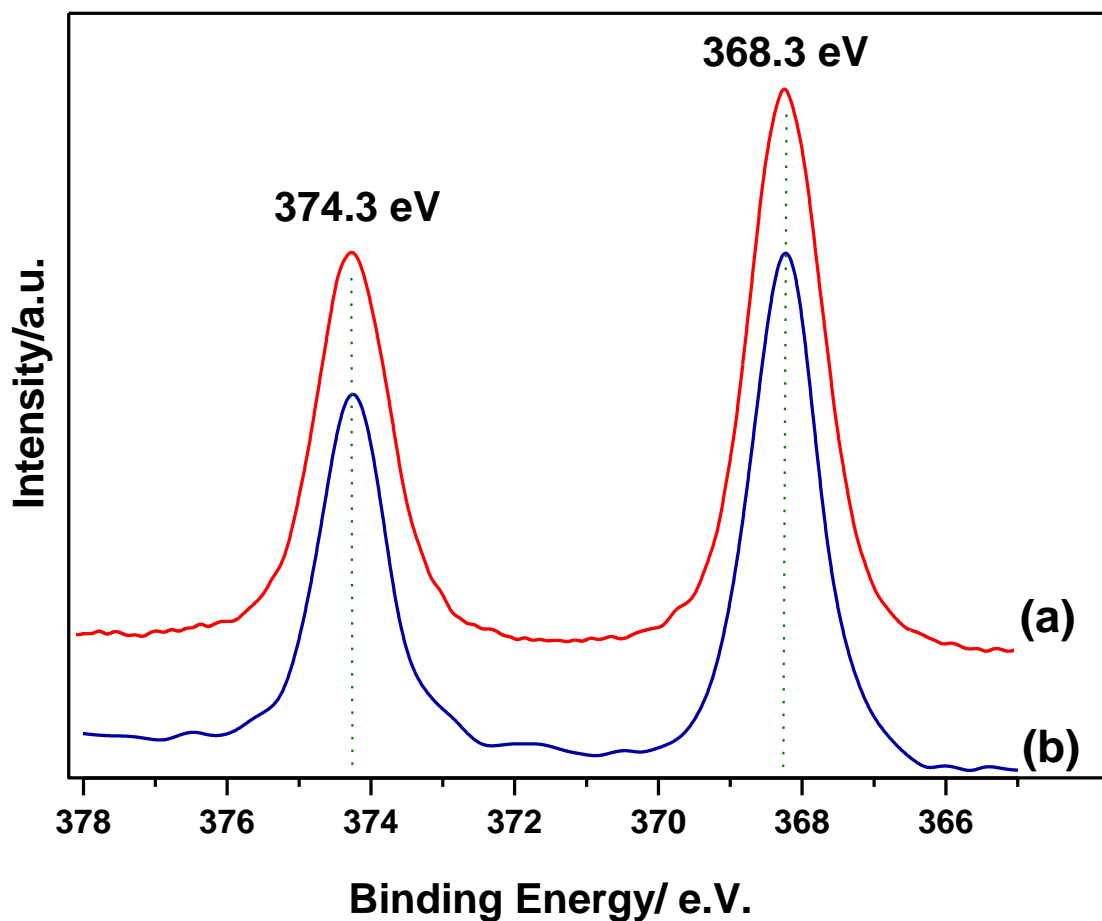
Fig. 2 Ag3d core-level spectra (XPS) of (a) fresh and (b) spent 1D Ag-Mn nano-rod catalyst.

To get insight details about the surface property, Raman spectroscopy (Figure 3) and FTIR-spectrum (Figure 5) analyses of the sample were conducted. Four major peaks were observed in the Raman spectrum. The strongest peak at 660 cm^{-1} and three peaks at 289 cm^{-1}, 321 cm^{-1}, and 374 cm^{-1} in the Raman spectrum are the indicative of symmetry stretching mode and out-

of-plane bending modes of Mn_3O_4 in the sample.[40] Moreover, the Raman spectrum of the spent catalyst was identical as that of the fresh catalyst, which beared consistency with the XRD and XPS results.
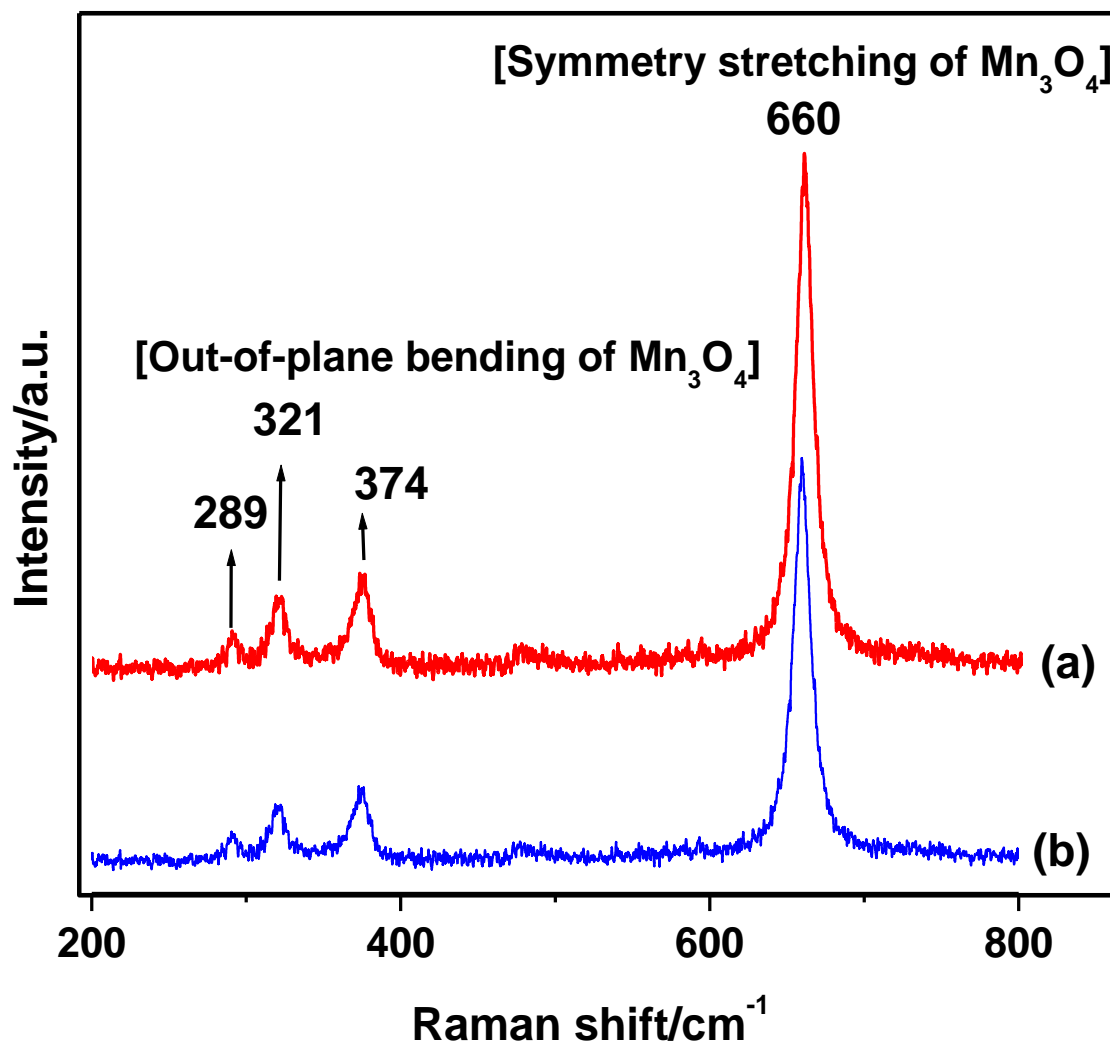
Fig. 3 Raman spectra of (a) fresh and (b) spent 1D Ag-Mn nano-rod catalyst.

SEM analyses were undergone to know the shape and morphology of the catalyst (Figure 4). Lower magnified SEM images revealed that the sample possesses thousands of throughout uniform nanorods and is devoid of aggregation. However, SEM image with higher magnification (Figure 4b) showed that diameter of each rod is with a diameter of ~ 20 nm and length of ~ 6 μm in length. The corresponding SEM-EDAX image (Figure S4, Supporting Information) further indicated the presence of Ag, Mn and O in the sample and no impurity like C, Br or N, which

demonstrated the exclusive expulsion of the surfactant upon calcinations. Moreover, from the SEM of the spent catalyst it is also visualized that there was no structural deformation after catalysis (Figure 4f).
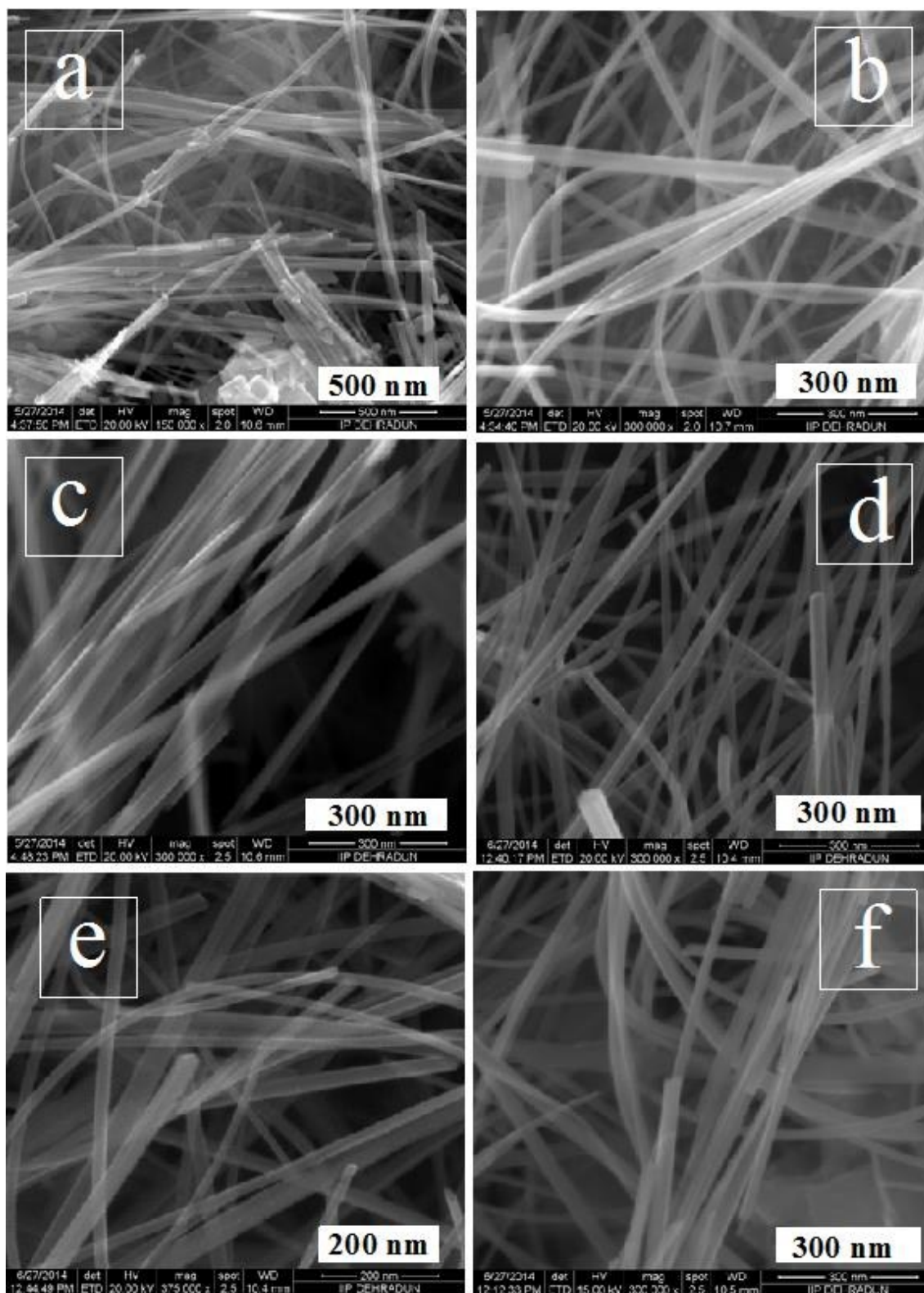
Fig. 4 SEM (a-e) images (at different magnifications) of fresh and that of (f) spent 1D Ag-Mn nano-rod catalyst.

10

This fact was further proved from the FTIR analyses of the uncalcined catalyst (Figure 5). In the uncalcined sample, the peaks observed at 812, 1062 cm^{-1} can be indexed to the C-N$^+$ stretching modes of CTAB molecules.[1] The peaks at 1378 and at 1462 cm^{-1} can be indexed to symmetric mode of vibration of the head groups of the methylene moiety (N$^+$—CH$_3$) and CH$_2$ scissoring mode respectively.[41,42] Above 1600 cm^{-1} to 3000 cm^{-1} are due to CH$_2$ symmetric and antisymmetric vibrations, respectively. Notably, the shift of vibrations to lower frequency observed as the alkyl chains faced hydrophobic environment in Ag-Mn blocks upon the surface of which the CTA-moieties were supposed to be bound.[41,42] It can be asserted that, the mutual interactions between CTAB and the Ag-Mn surface have taken place. Various bands were detected at 2800–3020 cm^{-1}, which can be attributed to the presence of CTAB. The FTIR spectrum of CTAB diplayed strong bands at 2918 and 2846 cm^{-1}, can be indexed to the asymmetric and symmetric stretching vibrations of C–CH in the methylene chains. The bands at 1450–1500 cm^{-1} occurred due to the deformation of –CH$_2$– and –CH, and the weak band at 3011 cm^{-1} as the C–CH$_3$ asymmetric stretching and N–CH symmetric stretching vibrations of the solid surfactant.[41,42] These frequencies were not observed when the substance (uncalcined catalyst) was calcined at 500 °C in air . It indicated that, the embedded CTAB moieties have been completely combusted from the catalyst surface during calcination. After calcinations, some new bands were visible in the FTIR-spectra of the catalyst (Figure 5a). The regions from 750–600 and 600–450 cm^{-1} correspond to the Mn–O stretching and bending vibrations. The Mn–O frequencies (lattice vibrations) occurred around 724 and 525 cm^{-1} in the spectrum was designative of a tetragonally distorted cubic lattice. These absorption were concerned with the coupling mode between Mn–O stretching modes of tetrahedral and octahedral sites.[43] The band at 612 and 509 cm^{-1} in the spectrum of the catalyst was assigned to Mn-O vibrations of bivalent manganese ions in tetrahedral co-ordination.[44] Moreover, it was also confirmed from the FTIR diagram that, there was no structural change in the catalyst even after 8 recycles.
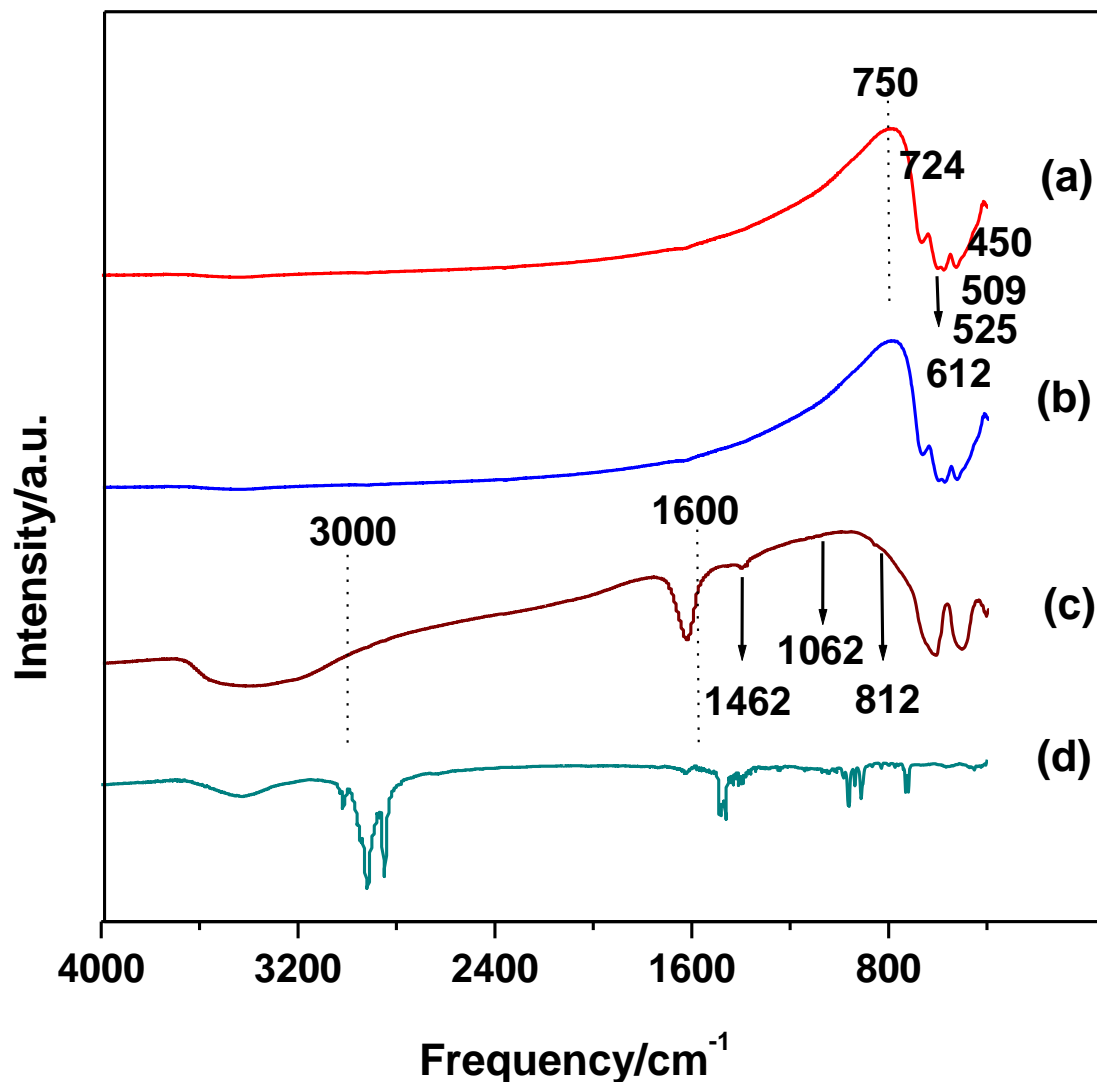
Fig. 5 FTIR spectra of (a) fresh, (b) spent, (c) uncalcined 1D Ag-Mn nano-rod catalyst and (d) that of cationic surfactant CTAB.

The TEM image in Figure 6a illustrates the network structure due to the assembly of finely grown flexible Ag-Mn nanorods. The magnified view in Figure 6c, 6d reveal that the rods are usually 30– 40 nm in diameter. The typical HRTEM image of the catalyst is shown in Figure 6e. HRTEM image displayed that the catalyst is composed of tiny silver nanoparticles of and are thoroughly dispersed on Mn_3O_4 nanorods (Figure 6e). Very few larger particles ($\sim$ 8nm) were also observed from the TEM image. The corresponding TEM histogram of showed that the

supported Ag nanoparticles with sizes between 2.5-6.5 nm (Figure 6c & Figure S5a, Supporting Information). Elaborately speaking around 1nm, 2nm, 3nm, 4 nm, 5 nm, 6 nm and 8nm range the calculated Ag particles were 2%, 15%, 40%, 15%, 18%, 6% and 4% respectively. The interplanar spacing of the lattice fringe distance of 0.28 nm indicates the (103) lattice spacing of Mn_3O_4[45] which was distinguished from of 0.23 nm corresponding to (111) plane of metallic Ag (Fig. 2h).[24-26] Although from SEM image, structural deformation was hardly visualized, but the TEM image of the spent catalyst showed that although the morphology of the catalyst was hardly undergone considerable change after eight reuses, but certain changes occurred in the silver particle size (and its size distribution) of the catalyst (Figure 6f & Figure S6b, Supporting Information). Elaborately, around 1nm, 2nm, 3nm, 4 nm, 5 nm, 6 nm, 8 nm and 10 nm range the calculated Ag particles were 2%, 15%, 35%, 18%, 15%, 7%, 6% and 2% respectively; the counted total number of Ag nanoparticles was 200 and basically reflected the accuracy of the average size of Ag nanoparticles. After eight reuses, probably, some of the Ag particles agglomerated and resulted in the formation of larger particles ($\geq$ 8nm), and this may be the possible reason for the lowering down the catalytic activity of the catalyst.

The thorough dispersion of silver (Ag), manganese (Mn) and oxygen (O) in the rod-like structure was confirmed from STEM-elemental mapping based on Figure 4a (Figure S6, Supporting Information). From the STEM-elemental mapping of Ag (Figure b, Supporting Information), presence of metallic silver and no sort of silver-oxide can be clearly visualized. Additionally, the SAED pattern showed a polycrystallinity of the catalyst, demonstrating that the nanorods are randomly orientated (Figure S7, Supporting Information). Moreover, the presence of (103) plane of Mn_3O_4 spinel and (111) and (220) plane of metallic Ag was clearly visualized from the TEM-SAED diagram.
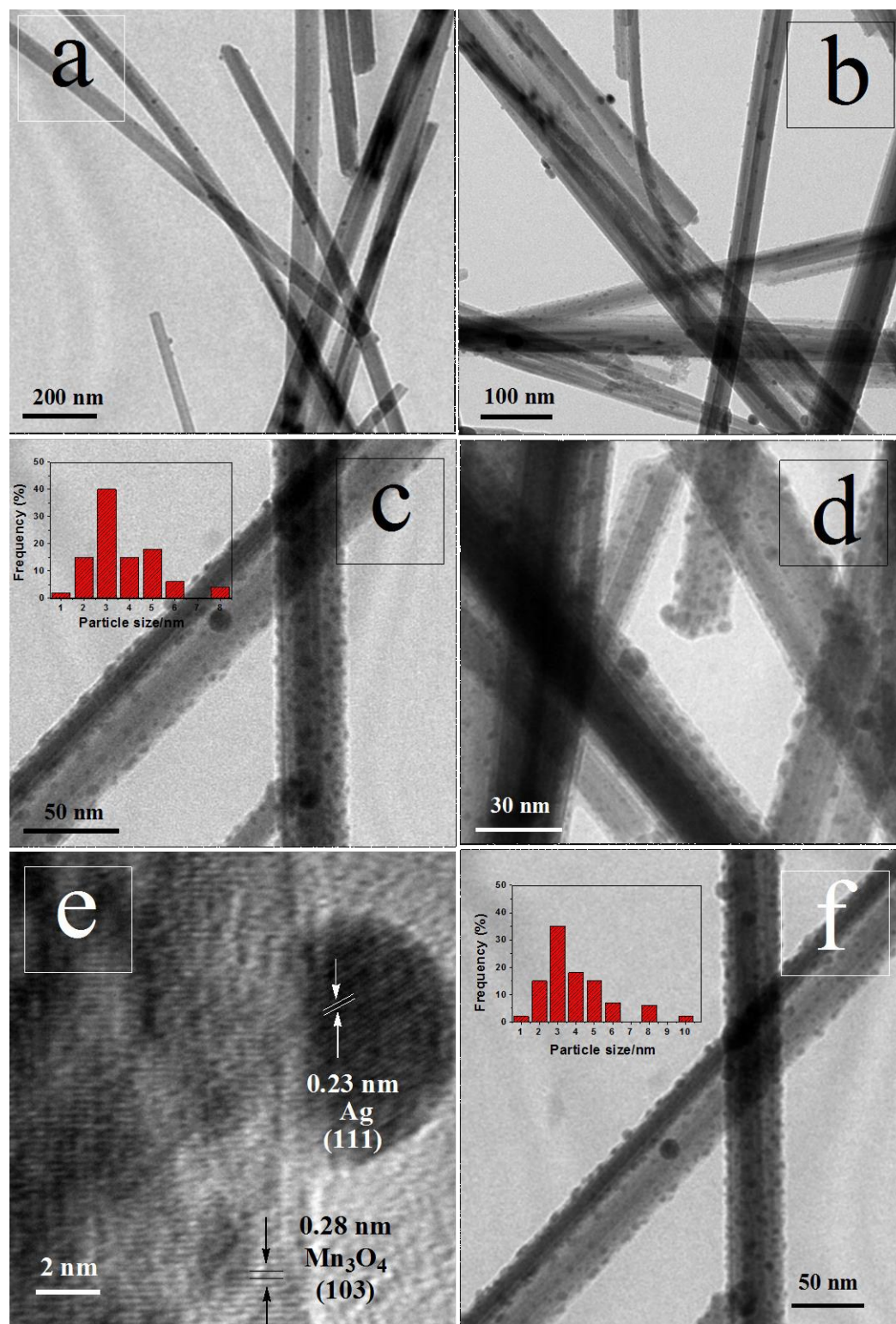
Fig. 6 TEM (a-e) images (at different magnifications) of fresh and that of (f) spent 1D Ag-Mn nano-rod catalyst.

Possible Formation Mechanism of 1D Nanostructures.

The formation of 1D Ag-Mn nanorods catalyst is interesting, though the thorough mechanism is unclear. To explore the formation mechanism of 1D Ag-Mn nanorods, various time-dependent hydrothermal experiments were performed and the final products were undergone SEM/TEM analyses. In the absence of CTAB, rather agglomerate particles were obtained instead of rods (Figure S8, Supporting Information). However, inhomogenous disperse rods with indefinite aspect ratio (marked with red) were generated when Ag: CTAB molar ratio was 1: 1 (Figure S9, Supporting Information); moreover agglomerates were also visualized apart from nanorods. This finding refelected the necessity of CTAB in contributing towards nanorods formation. Throughout uniform nanorods (devoid of agglomeration) was obtained only when Ag: CTAB = 1: 5 and the hydrothermal treatment time was 18h. That means, yield of nanorods increased with an increased concentration of CTAB, under autogeneous pressure. This experimental finding bears consistency with the previous reports.[46] When the hydrothermal treatment time was 6h, very few rods generated, rest of the sample was full of agglomeration, indicating the fact that, the rods grew slowly from these aggregates (Figure S10, Supporting Information). When the hydrothermal treatment time was 30h, non-uniform icosahedral-structures (with particle size 150-300 nm particle size) became the predominant (Figure S11, Supporting Information). However when TEM of selected areas of this sample was taken, it was observed that, there were very few rods attached with the wall of the icosahedral-structures, indicating the fact that, the nanorods assembled by means of Ostwald ripening process and ultimately results in this type of structure. It is noteworthy that, the cationic surfactant CTAB acts as "soft template" and facilitates self-assembly-mechanism.

It is pertinent to mention that, the growth of 1D Ag-Mn nanorods with high aspect ratio also depends on the amount of Ag used. It is a known fact that, without the use of Mn-precursor, formation of Ag-rods is possible.[47,48] We also confirmed this statement, when we prepared the sample without using any Mn-precursor and other conditions remained unaltered (SEM analyses, Figure 7a,b). But, if the reverse case is applied, i.e without taking Ag-precursor, or taking very less loading of Ag on Mn_3O_4 (0.9% loading), some irregular spherical type of

particles were formed (Figure 7c,d), reflecting the fact that, Ag-ions induce the nanorods-generation.
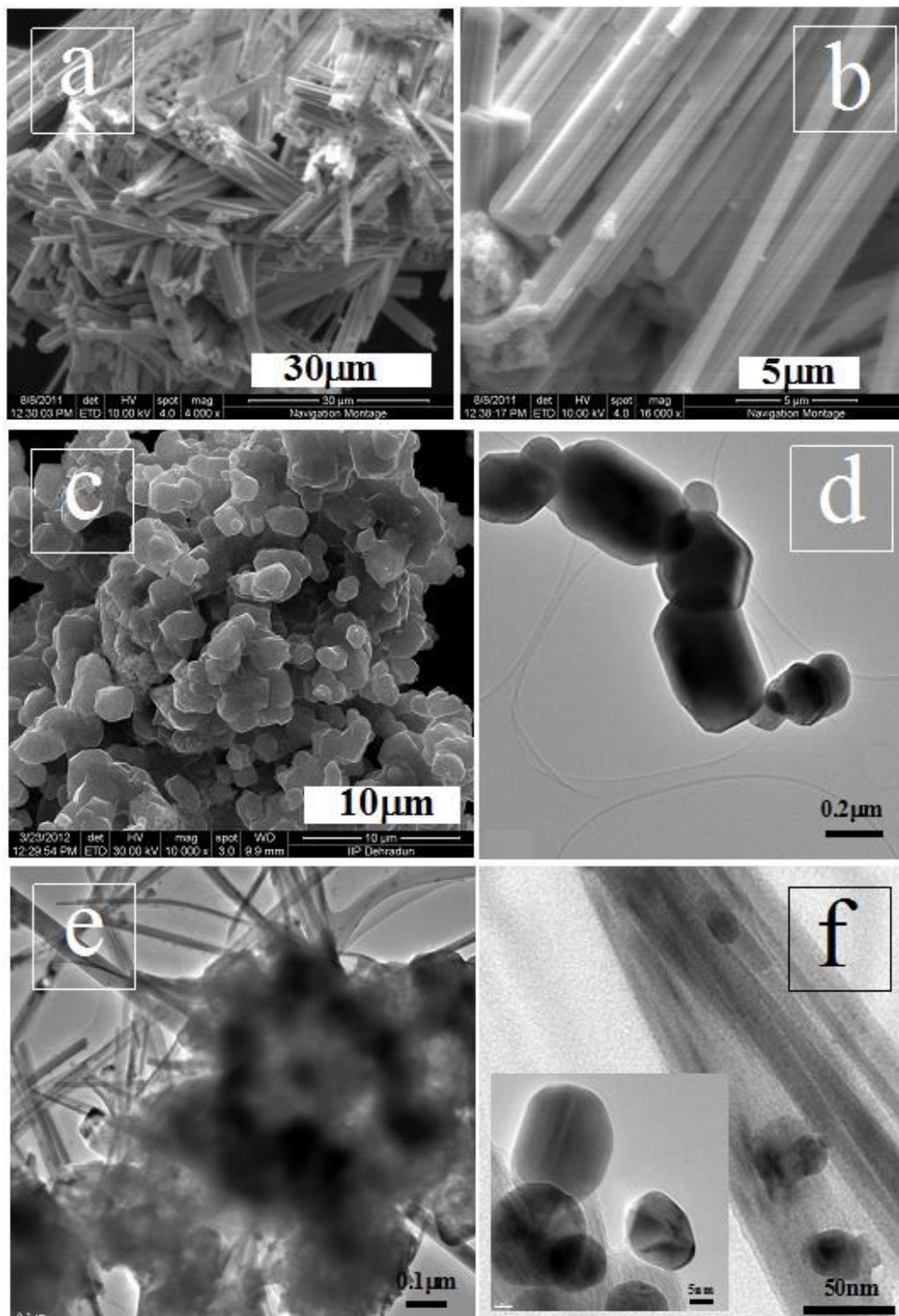
Fig. 7 (a,b) SEM image of the sample without using Mn-precursor, (c) SEM and (d) TEM image of the sample when loading of Ag is 0.9%, (e) TEM image of the sample when loading of Ag is 2.7%, and (f) TEM image of the sample when loading of Ag is 7.8%.

Moderate Ag loading (2.7% Ag) generates almost uniformly distributed rods with high aspect ratio and size of Ag nanoparticles are 2-5 nm and almost spherical in shape. Much more loading of Ag (7.8% Ag loading) doesnot change the overall morphology, instead, some larger Ag-particles with irregular shapes were formed (Figure 8f and 8f inset). From these experimental-observations, we can infer that, the whole process follows seed-mediated process.[47] As a cationic surfactant, CTAB completely ionized in water: Mn^{2+}, CTA^+, Ag^+ and anions OH^-, existed in basic solution.[49] Thus, self-assembly mechanism between ionic CTAB molecules and charged species is generated via electrostatic interaction in solution. The formation of almost spherical aggregates of nanoparticles may be brought from the high electrostatic attraction between positive CTA^+ cations and negative OH^- anions on the surface of nanoparticles as well as the hydrophobic interactions and van der Waals attraction caused by adjacent CTAB adsorbing on Ag-Mn nanoparticles. Elaborately speaking, in our synthetic procedure, the spherical micelles of $CTAB-Mn_3O_4^-$ were transformed into micelles with rod-shape, due to the result of attractive electrostatic interaction between the CTAB-stabilized negative manganese ions and the positive Ag^+ ions, where Ag^+ ions trigger symmetry-breaking anisotropic growth through selective adsorption onto particular crystal planes of Mn.[25] Thus, the decrement in surface energy of the Mn_3O_4 seed crystals in a particular direction gives birth to 1-D rodlike micellar structure, and this acts as the nucleating agent for the growth of the Mn_3O_4 nanorod. We observed that the amount of silver ions present in the solution has a pronounced influence on the nanorod growth. CTAB can influence surface energy of the system and thus control the nucleation rate of the Ag-Mn particles (CTAB-embedded). Initially, the surface energy of the system is isotropic and thus, almost spherical particles (although non-uniform) were obtained since they represent the lowest possible surface energy. Prolonged hydrothermal-time changes surface energy to be anisotropic and the particles aggregate into 1D nanostructures.[50]

It is noteworthy to mention that, when KMnO₄ was taken as the precursor of Mn, plate-like structures with non-uniform and larger particle size was obtained (Figure S12, Supporting Information).

Catalytic Oxidation Reaction. The reactions of the different catalyst for selective oxidation of cyclohexane are shown in Table 1.

Table 1. Activities of the Different Catalysts for Cyclohexane Oxidation [a]

Entry	Catalyst	C_C(%) [b]	S_P(%) [c]	Y_P(%) [d]	E_0 [e]
1	No Catalyst	-	-	-	-
2	Ag^{COM}	5	35	1.75	-
3	Ag$_2$O^{COM}	3.5	27	0.94	-
4	Mn$_3$O$_4^{COM}$	11.5	38	4.37	-
5	Ag$_2$O-Mn$_3$O$_4^{IMP}$	15	45	6.75	1.7
6[f]	AgMn$^{NR5.7}$	88	75	66	16.5
7[g]	AgMn$^{NR5.7}$	80	65.5	52.4	13.1
8[h]	AgMn$^{2.7}$	35	78	27.3	6.9
9[i]	AgMn$^{7.8}$	96	57	54.72	13.7
10[j]	AgMn$^{5.4}$	48	67	32.16	8

[a] Typical reaction conditions: solvent (MeCN) = 10 ml, substrate (cyclohexane) = 1g, catalyst= 0.1 g, cyclohexane: H₂O₂ (molar ratio) = 1:4, reaction temperature = 40 °C; time = 10 h. [b] C$_B$ = Conversion of cyclohexane based upon the FID-GC using anisole as external standard = [Moles

of cyclohexane reacted/initial moles of cyclohexane used] x 100. [c] S_P = Selectivity to cyclohexanone = [Moles of products produced/ moles of cyclohexane reacted] x 100. [d] Y_P = Yield of cyclohexanone= $C_C \times S_P/100$. [e] E_0 = H_2O_2 efficiency calculated by 100 ×moles of cyclohexanone formed/total moles of H_2O_2added; [f] fresh and [g] spent (after 8 recycles) Ag-Mn nanorods catalyst (Ag loading 5.7%), catalyst with Ag loading [h] 2.7%, [i] 7.8% and [j] 5.4% (using $KMnO_4$ as the precursor of Mn).

All the experiments were carried out at 40° C. Neat reaction (entry 1, Table 1) was performed, but conversion of cyclohexane was too poor to be detected in GC. The prepared 1D Ag-Mn nanorods catalyst (AgMn$^{NR5.7}$) showed better catalytic efficiency compared to the commercial catalysts (entry2-4, Table 1) and even better than Ag-Mn catalyst prepared in the impregnation method (Ag$_2$O-Mn$_3$O$_4$^{IMP} entry 5, Table 2.), which indicated the necessity of the present catalytic system. Furthermore, the commercial Mn_3O_4 spinel (whose particles are of larger size and not uniform) diplayed poor activity compared to our so prepared 1D Ag-Mn nanorods catalyst. We also studied the activity of 1D Ag-Mn nanorods catalyst catalyst with different cyclohexane: H_2O_2 molar ratio. When the molar ratio of cyclohexane: H_2O_2 was 1:1 or 1: 2.5, the conversion of cyclohexane was very low (Figure 8), which indicated the decomposition of H_2O_2 in that temperature.
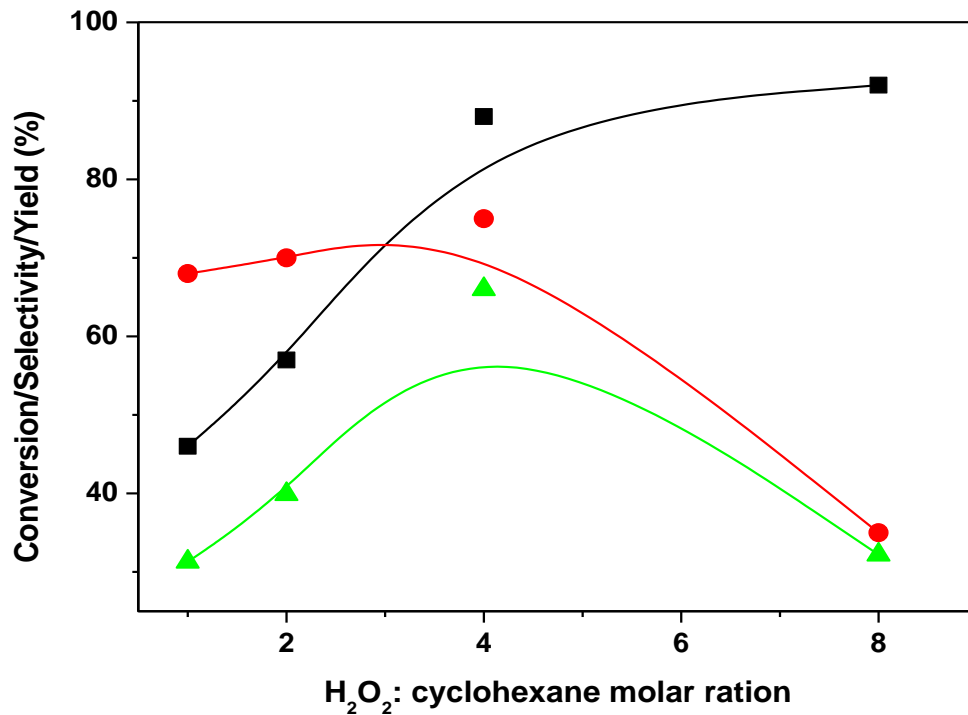
Fig. 8 Effect of H_2O_2: cyclohexane molar ratio on cyclohexane oxidation.

[■] Conversion of cyclohexane;   [●] Selectivity to cyclohexanone; [▲] Yield of cyclohexanone.

Reaction Condition: cyclohexane =1g; catalyst = 0.1g; temperature = 40° C; time= 15 h.

Keeping all the optimum conditions unhindered, when the catalytic oxidation of cyclohexane was carried out for hours, we speculated the increment of conversion of cyclohexane, as well as selectivity of cyclohexanone with time (Figure 9).
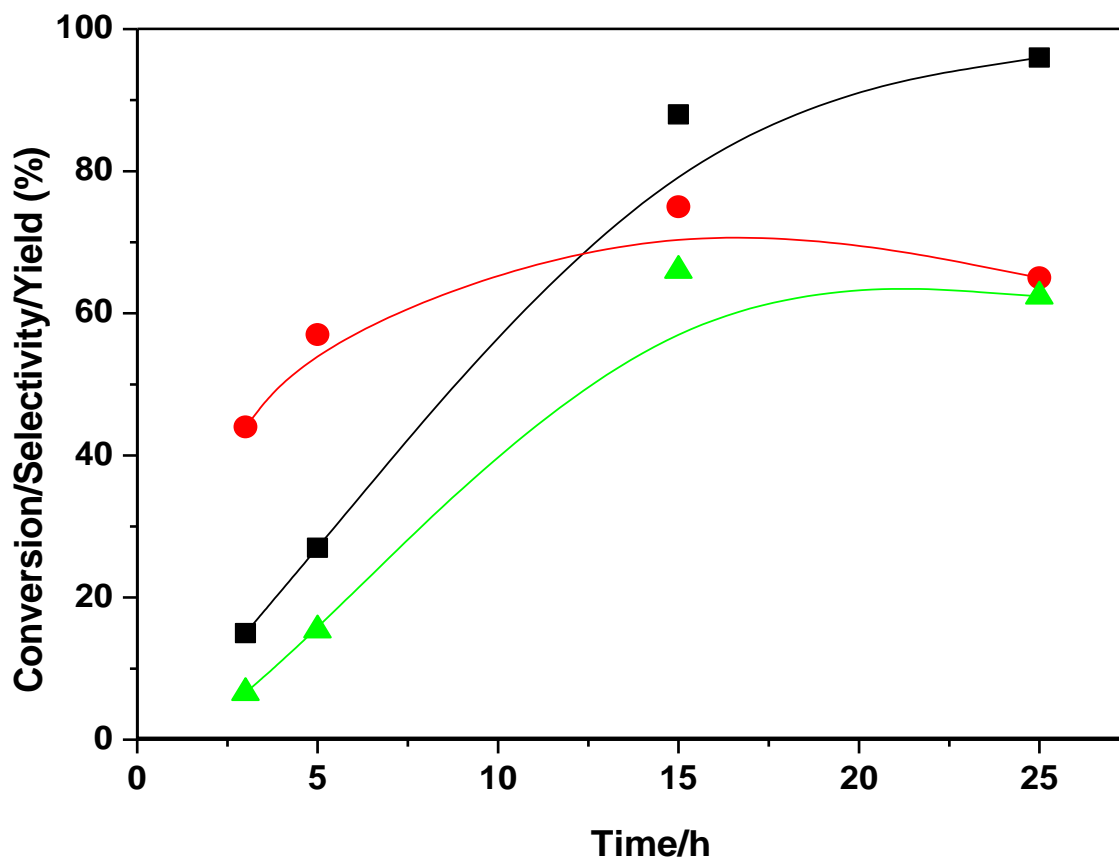
Fig. 9 Effect of time on cyclohexane oxidation.

[■] Conversion of cyclohexane; [●] Selectivity to cyclohexanone; [▲] Yield of cyclohexanone.

Reaction Condition: cyclohexane =1g; catalyst = 0.1g; cyclohexane: H_2O_2 mole ratio =1:4; temperature = 40° C.

But after 10 h, although higher conversion of cyclohexane was observed, but selectivity to cyclohexanone decreased owing to the formation of cyclohexanediol. The corroboration of all investigations demonstrated that the spinel phase of Mn (i.e. Mn_3O_4) as well as small particle size of Ag (supported on Mn_3O_4 nanorods) determines the reactivity of the 1D Ag-Mn nanorods catalyst. Loading of Ag on Mn_3O_4 also plays an important role in cyclohexane oxidation. Ag loading 5-6% proved to be optimum for maximum yield of cyclohexanone. Lower Ag loading

(entry 8, Table 1) led to very low conversion of cyclohexane, indicating the role of quantitative amount of supported metallic Ag; higher Ag loading (entry 9, Table1), although led to higher conversion of cyclohexane, but selectivity to cyclohexanone decreased sharply due to the formation of unwanted by-products.

It is noteworthy to mention that, E_0 value calculated were found to be 16.5 and 13.1, when fresh and spent catalyst (after 8 catalysis) were used, respectively (Table 1). These values are quite larger than those of the other catalysts, which indicated the fact that, these catalysts (Ag-Mn catalysts, where loading of Ag is 5.7%) utilized H_2O_2 quite well to achieve the desired products.

We also conducted the same experiment using Ag-Mn catalyst (prepared using $KMnO_4$) with plate-like morphology (Ag-Mn[PL5.4], Entry 10, Table 1) and noticed that, it showed comparatively lesser activity than the rod-like structures despite of same metal loading (5.4 %) and similar BET surface areas (37 m^2/g). This experimental finding was in accordance with the fact that, a higher dispersion of Ag (ultra small) anchored on the Mn_3O_4 spinel rods (support) and the synergy displayed between them was the key of the catalyst-efficacy. Depending on this hypothesis, we can infer that, Ag-Mn catalyst with nanorod-like structures is much more reactive than the other structures. This phenomenon is demonstrative of the significant activity dependence on the morphology of the Ag-Mn catalyst. The morphology of the nanorods serve suitable dispersion of the catalyst particles in solution, in comparison with the large aggregates of particles with indefinite morphology.[51]

Commercial catalysts and even Ag/Mn_3O_4 catalyst prepared by impregnation method didnot show any appreciable activity in oxidation of cyclohexane. These results reflected to the non-uniform and irregular shape/sizes of these catalysts, which limit their catalytic performances. Furthermore, ultrasmall Ag nanoparticles supported on 1D Mn_3O_4 nanorods prepared in our method displayed high efficacy in production of cyclohexanone from cyclohexane, due to the synergistic interaction occurred between these two catalytic species. Moreover, this strong synergism also prevents the Ag nanoparticles to be leached out from catalyst.

Reusability test.

The true heterogeneous nature of the catalyst was examined in terms of the recyclability and stability. After completion of the reaction, the catalyst was filtered (hot filtration process) and was dried for 12h at 100° C. The used catalyst was introduced newly and subsequently 8 times to carry out the catalytic oxidation. The reusability-test of the 1D Ag/Mn₃O₄ catalyst was studied without further regeneration of the catalyst and unhindering experimental conditions. The catalyst showed 65.5% selectivity even after 8 subsequent runs (entry 7, Table 1 & Figure 10).
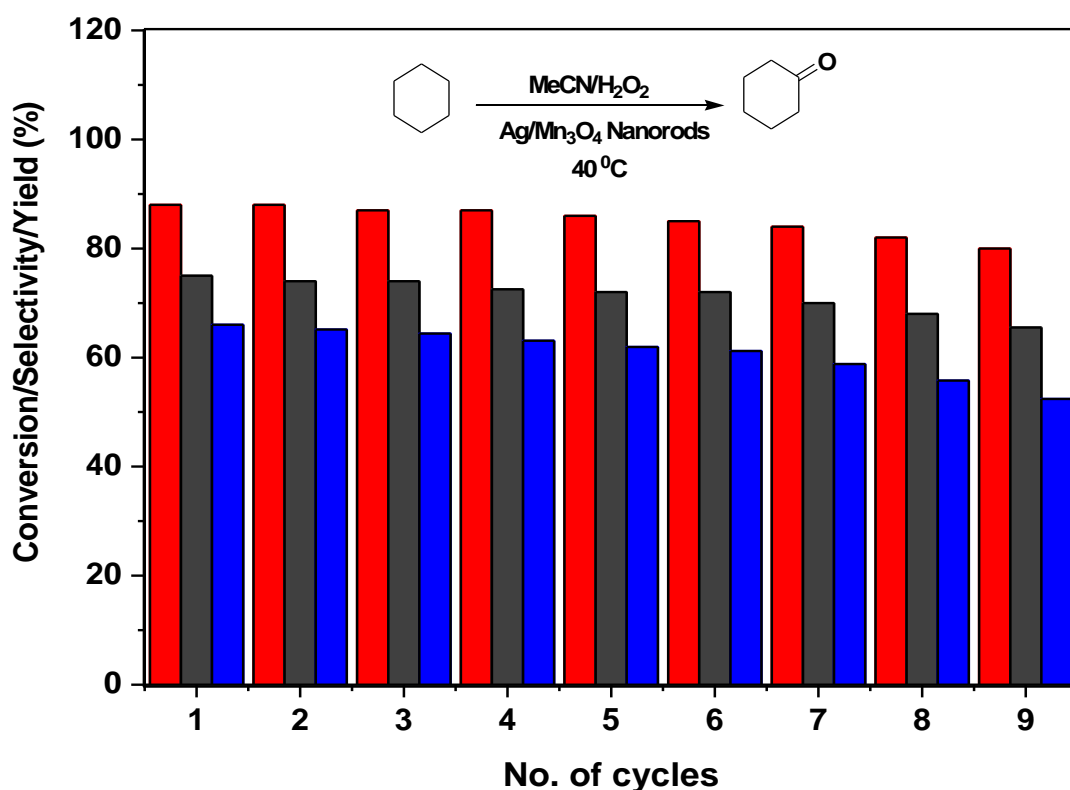
Fig. 10 Reusability test on cyclohexane oxidation.

[■] Conversion of cyclohexane;   [■] Selectivity to cyclohexanone; [■] Yield of cyclohexanone.

Reaction Condition: cyclohexane =1g; catalyst = 0.1g; cyclohexane: H_2O_2 mole ratio =1:4; temperature = 40° C; time = 15h.

Importantly, leaching of the metal(s) was not observed during this reaction as ascertained by ICP-AES analysis of the obtained filtrates during the recycling experiments. We carried out ICP-AES of the spent catalyst and compared the results with that of the fresh one. We noticed that the percentage of Ag and Mn present in the spent catalyst (after 8 recycles, <2 ppb) was approximately same to that of the fresh catalyst (as confirmed by ICP-AES). Moreover, thorough characterization of the spent catalyst was carried out by XRD, XPS, SEM, TEM, FTIR and Raman spectroscopy. All of these characterization data were in consistent with the fact that, the catalyst retained its structure even after eight reuses, establishing that there was no leaching and the reaction was of true heterogeneity.

CONCLUSIONS

In conclusion, we reported a facile preparation of utrasmall Ag nanoparticles supported on Mn_3O_4 spinel with a unique one-dimensional structure. The investigation showed that, it was a 2-stage trajectory, where nanoparticles were generated initially, followed by organized assembly of these nanoparticles into nanorods. It was possible to tune the morphology of the Ag-Mn composites varying the synthetic parameters. This preparation-method could easily be scaled up due to its simplicity. Moreover the high thermal stability and reusability of the catalyst and its excellent ability in oxidation of cyclohexane to cyclohexanone using H_2O_2 as oxidant and may be a potential alternative path of the conventional process.

REFERENCES

1. K. An, S. Alayoglu and G. A. Somorjai, *Nano Lett.,* 2012, **12**, 5196 –5201.

2. M. Jin, H. Zhang, Z. Xie and Y. Xia, *Energy Environ. Sci.,* 2012, **5**, 6352 –6357.

3. F. Zaera, *ChemSusChem,* 2013, **6**, 1797–1820.

4. J. D.Holmes, K. P.Johnston, R. C.Doty and B. A. Korgel, *Science*, 2000, **287**, 1471–1473.

5. B. Goris, S. Bals, W. Van den Broek, E. Carbó-Argibay, S. Gómez-Graña, L. M. Liz-Marzán and G. Van Tendelo, *Nature Mater.*, 2012, **11**, 930–935.

6. W. Lueangchaichaweng, N. R.Brooks, S. Fiorilli, E. Gobechiya, K. Lin, L. Li, S. Parres-Esclapez, E. Javon, S. Bals, G. V. Tendeloo, J. A. Martens, C. E. A. Kirschhock, P. A. Jacobs and P. A. Pescarmona, *Angew. Chem.,* 2014, **53**, 1585–1589.

7. C. Jiang, S. Liu, X. Chen and S. Yu, *CrystEngComm.,* 2014, **16**, 8646–8651.

8. X. D.Wang, J. H. Song, J. Liu and J. L.Wang, *Science*, 2007, **316**, 102–105.

9. Y. Qin, X. D. Wang and Z. L. Wang, *Nature*, 2008, **451**, 809–813.

10. Z. W. Pan, Z. R. Dai and Z .L. Wang, *Science*, 2001, **291**, 1947–1949.

11. Y. Li, J. Wang, Z. Deng, Y. Wu, X. Sun, D. Yu and P. Yang, *J. Am. Chem. Soc.,* 2001, **123**, 9904–9905.

12. M. Mo, J. Zeng, X. Liu, W. Yu, S. Zhang and Y. Qian, *Adv. Mater.,* 2002, **14**, 1658–1662.

13. X. W. Xie and W.J.Shen, *Nanoscale*, 2009, **1**, 50–60.

14. X. Liu, A. Klust, R. J. Madix and C. M.Friend, *J. Phys. Chem. C,* 2007, **111**, 3675–3679.

15. J. Lu, J. J. Bravo-Suárez, A. Takahashi, M. Haruta and S. T. Oyama, *J. Catal.,* 2005, **232**, 85–95.

16. Y. Lei, F. Mehmood, S. Lee, J. Greeley, B. Lee, S. Seifert, R. E. Winans, J. W. Elam, R. J. Meyer, P. C. Redfern, D. Teschner, R. Schlögl, M. J. Pellin, L. A. Curtiss and S. Vajda, *Science,* 2010, **328,** 224–227.

17. J. Mao, G. Zhao, D. Wang and Y. Li, *RSC Adv.,* 2014, **4**, 25384–25388.

18. Y. Dai, S. Tang, S. Vongehr and X. Meng, *ACS Sustainable Chem. Eng.,* 2014, **2**, 692–698.

19. R. Xu, X. Wang, D. S. Wang, K. B. Zhou and Y. Li, *J. Catal.,* 2006, **237,** 426–430.

20. Y.Liu, X.Li, C.Shi, J.Liu, A.Zhu and B.W.L.Jang, *Catal. Sci. Tech.,* 2014, **4,** 2589–2598.

21. Z. Qu, Y. Bu, Y. Qin, Y. Wang and Q. Fu, *Appl. Catal. B,* 2013, **132,** 353–362.

22. S. S. Acharyya, S. Ghosh, S. K. Sharma and R. Bal, *RSC Adv.,* 2015, **5**, 89879–89887.

23. B. Sarkar, R. K. Singha, R. Tiwari, S. Ghosh, S. S. Acharyya, C. Pendem, L. N. S. Konathala and R. Bal, *RSC Adv.,* 2014, **4,** 5453–5456.

24. S. Ghosh, S. S.Acharyya, S. Adak, L. N. S.Konathala, T. Sasaki and R. Bal, *Green Chem.,* 2014, **16,** 2826–2834.

25. S. Ghosh, S. S.Acharyya, R. Tiwari, B. Sarkar, R. K. Singha, C. Pendem, T. Sasaki and R. Bal, *ACS Catal.,* 2014, **4,** 2169–2174.

26. S. Ghosh, S. S. Acharyya, D. Tripathi and R. Bal, *J. Mater. Chem. A,* 2014, **2**, 15726–15733.

27. R. A. Sheldon and J .K. Kochi, Academic Press, New York, 1981.

28. R. Kumar, S. Sithambaram and S. L.Suib, *J. Catal.,* 2009, **262,** 304–313.

29. L. Liu, Y. Li, H. Wei, M. Dong, J. Wang, A. M. Z. S lawin, J. Li, J. Dong and R. E. Morris, *Angew. Chem.,* 2009, **121,** 2240–2243.

30. M. T. Musser, Ullmann's Encyclopedia of Industrial Chemistry, Wiley-VCH Verlag, Weinheim, 2007.

31.   A. A. White, M. S. Platz, D. M. Aruguete, S. L. Jones, L. D. Madsen and R. D. Wesson, *ACS Sustainable Chem. Eng.* 2013, **1,** 871–877.

32.   A. Bellifa, A. Choukchou-Braham, C. Kappenstein, L. Pirault-Roy, *RSC Adv.,* 2014, **4,** 22374–22379.

33.   (a) U. R. Pillai and E. Sahle-Demessie, *New J. Chem.,* 2003, **27**, 525–528; (b) O. Perraud, A. B. Sorokin, J. P. Dutasta and A. Martinez, *Chem. Commun.,* 2013, **49**, 1288–1290; (c) S. A. C. Carabineiro, L. M. D. R. S. Martins, M. Avalos-Borja, J. G. Buijnsters, A. J. L. Pombeiro, J. L. Figueiredo, *Appl. Catal. A: Gen*, 2013, **467,** 279–290; (d) M. Peixoto de Almeida, L. M. D. R. S. Martins, S. A. C. Carabineiro, T. Lauterbach, F. Rominger, A. S. K. Hashmi, A. J. L. Pombeiro and J. L. Figueiredo, *Catal. Sci. Technol.,* 2013, **3**, 3056–3069; (e) L. M. D. R. S. Martins, M. P. de Almeida, S. A. C. Carabineiro, J. L. Figueiredo and A. J. L. Pombeiro, *ChemCatChem*, 2013, **5**, 3847–3856.

34.   (a) G. Sankar, R. Raja and J. M. Thomas, *Catal. Lett.,* 1998, **55,** 15–23; (b) B. Modén, B. Z. Zhan, J. Dakka, J. G. Santiesteban and E. Iglesia, *J. Catal.,* 2006, **239,** 390–401.

35.   B. Sarkar, P. Prajapati, R. Tiwari, S. Ghosh, S. S. Acharyya, C. Pendem, R. K. Singha, L. N. S. Konathala, J. Kumar, T. S asaki and R. Bal, *Green Chem.,* 2012, **14,** 2600–2606.

36.   S. S. Acharyya, S. Ghosh, S. Adak, D. Tripathi and R. Bal, *Catal.Commun.,* 2015, **59,** 145–150.

37.   D. C. Lim, I. Lopez-Salido and Y. D. Kim, *Surf. Sci.* 2005, **598**, 96–103.

38.   D. Wang, Y. Li, Q. Wang and T. Wang, *Eur. J. Inorg. Chem.,* 2012, 628– 635.

39.   Z. Y. Tian, P. M. Kouotou, N. Bahlawane and P. H. T. Ngamou, *J. Phys. Chem. C,* 2013, **117**, 6218–6224.

40.   (a) F. Buciuman, F. Patcas, R. Craciun and D. R. T. Zahn, *Phys. Chem. Chem. Phys.,* 1999, **1**, 185–190; (b) Y. F. Han, F. Chen, Z. Zhong, K. Ramesh, L. Chen and E. Widjaja, *J. Phys. Chem. B,* 2006, **110**, 24450-24456.

41.   W. Cheng, S. Dong and E. Wang, *Langmuir,* 2003, **19**, 9434–9439.

42. S. S. Acharyya, S. Ghosh and R. Bal, *ACS Appl. Mater. Interfaces,* 2014, **6**, 14451–14459.

43. C. M. Julien, M. Massot and C. Poinsignon, *Spectrochim. Acta Part A,* 2004, **60**, 689–700.

44. J. Mondal, P. Borah, S. Sreejith, K. T. Nguyen, X. Han, X. Ma and Y. Zhao, *ChemCatChem.,* 2014, **6**, 3518–3529.

45. H. Wang, L. F. Cui, Y. Yang, H. S. Casalongue, J. T. Robinson, Y. Liang, Y. Cui and H. Dai, *J. Am. Chem. Soc.,* 2010, **132**, 13978 –13980.

46. N. R. Jana, L. Gearheart and C. J. Murphy, *J. Phys. Chem. B,* 2001, **105**, 4065–4067.

47. C. J. Johnson, E. Dujardin, S. A. Davis, C. J. Murphy and S. Mann, *J. Mater. Chem.,* 2002, **12**, 1765–1770.

48. R. E. Lamont and W. A. Ducker, *J. Am. Chem. Soc.,* 1998, **120**, 7602–7607.

49. D. P. Dubal, D. S. Dhawale, R. R. Salunkhe and C. D. Lokhande, *J. Electrochem. Soc.,* 2010, **157**, A812–A817.

50. Y. Li, J. Wang, Y. Zhang, M. N. Banis, J. Liu, D. Geng, R. Li and X. Sun, *J. Colloid Interface Sci.* 2012, **369,** 123–128.

51. G. Stoica, M. Santiago, P. A. Jacobs, J. Prez-Ramrez and P. P. Pescarmona, *Appl. Catal. A,* 2009, **371**, 43–53.

Fabrication of Ag Nanoparticles Supported on One-Dimensional (1D) Mn₃O₄ Spinel Nanorods for Selective Oxidation of Cyclohexane at RoomTemperature

Shankha Shubhra Acharyya, Shilpi Ghosh, Sachin Kumar Sharma and Rajaram Bal*

*Catalytic Conversion & Processes Division, CSIR-Indian Institute of Petroleum, Dehradun - 248005, India. Fax: +91 135 2660202; Tel: +91135 2525 917; E-mail: raja@iip.res.in

Silver nanoparticles supported on spinel Mn₃O₄ nanorods efficiently cyclohexane to cyclohexanone with high yield at room-temperature.